Remote Sensing Applications: Society and Environment 39 (2025) 101716



Contents lists available at ScienceDirect

Remote Sensing Applications: Society and Environment

journal homepage: www.elsevier.com/locate/rsase





Integrated aeromagnetic and remote sensing analysis for structural mapping in the El-Barramiya-Dungash region, Eastern Desert, Egypt

Mohamed Abdelrady [a,b,*], Luan Thanh Pham [c,**], Ferenc Molnár [a], Ali Shebl [d,e]

[a] Department of Mineralogy, Institute of Geography and Earth Sciences, Eötvös Loránd University, Budapest, 1117, Hungary
[b] Geology Department, Faculty of Science, Assiut University, Assiut, 71516, Egypt
[c] University of Science, Vietnam National University, Hanoi, Viet Nam
[d] Department of Geology, Tanta University, Tanta, 31527, Egypt
[e] Department of Mineralogy and Geology, University of Debrecen, Egyetem tér 1, 4032, Debrecen, Hungary

ARTICLE INFO

Keywords:
Aeromagnetic data
El-Barramiya-Dungash area
Edge filters
Lineaments
Subsurface structures
Textural analysis
PALSAR data
Euler deconvolution

ABSTRACT

The El-Barramiya-Dungash region in Egypt's Central Eastern Desert, is very rich in minerals and metals that has a significant part posting the economy of the country. This study integrates aeromagnetic data with textural analysis of ALOS PALSAR data to map structural features of the El-Barramiya-Dungash region. We apply some edge detecting techniques like the modified theta map (MTM), tilt angle of the horizontal gradient (TAHG), horizontal gradient of the second tilt derivative (HGSTDR), fast sigmoid detector (FS), enhanced horizontal gradient amplitude (EHGA), and balanced gradient amplitude (BHG) to aeromagnetic data to identify the underlying structures that are concealed beneath geological formations of the area. The findings show that all methods are able to give high resolution results, but utilizing the TAHG, FS, EHGA and BHG can avoid creating false edges. Four main tectonic trends including NNE-SSW, NE-SW, NW-SE, N-S and E-W are identified by analyzing the lineaments obtained from filtered aeromagnetic maps statistically. In addition, we also apply the Euler deconvolution (EUL) method to aeromagnetic anomalies of the area, where the results show that most magnetic structures are located between 123 and 850 m under the surface. Textural analysis, employing techniques such as Second Moment and Dissimilarity, effectively differentiated lithologies and delineated prominent structural trends, coinciding with aeromagnetic data findings. The findings also show that the determined lineaments according to Egypt's tectonic structure, correlate to the Gulf of Aqaba, Najd fault system, and Nubian trend (East African trend). These findings demonstrate the significant potential of the applied techniques for enhancing geological understanding and guiding future mineral exploration efforts.

* Corresponding author. Department of Mineralogy, Institute of Geography and Earth Sciences, Eötvös Loránd University, Budapest, 1117, Hungary.
** Corresponding author.
E-mail addresses: moh200@student.elte.hu (M. Abdelrady), luanpt@hus.edu.vn (L.T. Pham).

https://doi.org/10.1016/j.rsase.2025.101716
Received 20 February 2025; Received in revised form 4 August 2025; Accepted 3 September 2025
Available online 11 September 2025
2352-9385/© 2025 The Authors. Published by Elsevier B.V. This is an open access article under the CC BY-NC license (http://creativecommons.org/licenses/by-nc/4.0/).

1. Introduction

Various types of rocks have various magnetic characteristics, which can cause local or regional anomalies (disturbances) in the Earth's magnetic field. Magnetic data is considered one of the most important sources of information that can be used in mapping geological structures and lineaments, and exploration of mineral and water resources (Ejiga et al., 2019; Issa et al., 2021; Essa et al., 2022; Obiora et al., 2022; Arafa-Hamed et al., 2023; Lghoul et al., 2023; Alrefaee and Soliman, 2023; Hussien, 2023; Toushmalani et al., 2024; Embaby et al., 2024; El Saeed et al., 2024; Abdelwahed et al., 2024; Elhussein et al., 2024; Abubakar et al., 2024; Ghoneim et al., 2024). There are several advantages of aeromagnetic survey, which include deep exploration depths, low cost, high efficiency, and practicability in large-scale operations (Nabighian et al., 2005). For the purpose of the identification of geological structures, several authors have employed magnetic and other geophysical methods (Ekinci et al., 2014, 2020; Saleh et al., 2018; Said, 1962; Abdelazeem et al., 2019; Fu et al., 2020; Raju and Kumar, 2020; Zhdanov, 2021; Saada et al., 2021a, 2022, 2025; Gobashy et al., 2022; Mohamed et al., 2022; b, c; Kassia et al., 2023; Abdelrady et al., 2023, 2024; Abdelrady et al., 2023a,b; Hamimi et al., 2023; Eldosouky et al., 2022a, 2022b, 2024a, 2024b). Recently, there has been extensive use of aeromagnetic data in the search for mineral resources. It has been demonstrated that aeromagnetic data is effective and capable of locating hydrothermal alteration sequences connected to mineral deposits (Abdelkader, 2024; Badawi and et al., 2022; Shebl, 2021). Aeromagnetic information allows for the identification of changed zones associated with porphyry minerals as well as the delineation of structural patterns that act as conduits for hydrothermal alteration. The location of edges and the depths of magnetic rocks that create anomalies in the magnetic field have been defined using a range of techniques (Saada, 2016; Sehsah et al., 2019; Sehsah and Eldosouky, 2020; Eldosouky and Saada, 2020; Abudeif et al., 2023; Oliveira et al., 2023; Othman et al., 2024; Eldosouky et al., 2025). Numerous ways exist for extracting sources, as well as the majority of them rely on the field's vertical or horizontal derivatives (Jorge, 2023; Kamto, 2023; Pham and Prasad, 2023; Aprina, 2024; Pham et al., 2025). The first filters, including the horizontal gradient (HG), total gradient (TG), tilt angle (TA), and theta (TM) offer useful information on source locations but frequently are unable to clearly distinguish the edges (Grauch and Cordell, 1987; Roest et al., 1992; Miller and Singh, 1994; Wijns et al., 2005). Many improved filters are designed for identifying the limits of potential sources (Prasad et al., 2022; Pham, 2024a, 2024b). Ferreira et al. (2013) improved the edges by using TAHG. Chen et al. (2017) used MTM to improve the resolution of the edges in the TM map. Nasuti et al. (2019) introduced HGSTDR to provide high-resolution edges. Oksum et al. (2021) presented FS that uses the fast sigmoid and derivatives of the gradient amplitude to outline the edges. Pham et al. (2022a) used the EHGA method to bring the sharp signals over the edges. Prasad et al. (2022) introduced BHG, which provides the edges with the same amplitude in the output maps.

Remote sensing data, when integrated with aeromagnetic data, provides a powerful framework for delineating structural elements that control hydrothermal alteration zones across diverse terrains (Abdelkader, 2024; Abo Khashaba, 2023; Araffa and et al., 2022; Hegab, 2022; Shebl, 2023). Remote sensing excels in providing a synoptic overview of vast regions with many different applications (Thao et al., 2023; Duong et al., 2024; Liem et al., 2025), facilitating the identification of major and regional structural trends through judicious interpretation and the application of appropriate analytical techniques (Eldosouky et al., 2022c, 2024a; Alarifi et al., 2024). Among these techniques, textural analysis emerges as a valuable tool for discerning structural features. Unlike spectral analysis, which primarily focuses on spectral signatures, textural analysis examines tonal variations and spatial relationships between neighboring pixels (Haralick, 1979; Shebl and et al., 2024). This approach unlocks a wealth of information, particularly regarding the inherent structural characteristics of the image. This enhanced information extraction stems from the inherent binary nature of pixel attributes within the textural analysis framework, where each pixel is characterized by its local variability and spatial context (Li, 2011).

The Central Eastern Desert's El-Barramiya-Dungash region has been the subject of several geological, geochemical, ASTER data, and geophysical research (e.g., Gad and Kusky, 2006; Salem et al., 2016; Saleh et al., 2018; Ghazala et al., 2021; Abdelrady, 2021; Mohamed et al., 2022; Abdelrady et al., 2023a,b; Abdelrady et al., 2023a,b; Shebl, 2021). Prior magnetic studies in the area used filtering techniques such as tilt derivative, first-order vertical gradients, gradient amplitude, peak detection, total gradient (or analytical signal), and center for exploration targeting (CET), which also included textural analysis and circular feature transform plugins (Saleh et al., 2018; Mohamed et al., 2022; Abdelrady et al., 2023a,b). However, recent studies pointed out that these methods are less successful in describing the deep sources or cannot detect all the edges of magnetic sources (Eldosouky et al., 2022a, 2022b; Pham et al., 2022b, 2023b; Abdelrady et al., 2024).

The goal of this study is to discover underlying geologic features in the El-Barramiya-Dungash area, which may be significant for future mineral development by applying recent techniques to aeromagnetic anomalies and textural analysis to ALOSPALSAR data. To pinpoint the source edges, we employ filterings such as the MTM, TAHG, HGSTDR, FS, EHGA and BHG. We also use the EUL method to determine the depths of the underground structures in the area.

2. Geologic setting

Egypt's Precambrian basement complex covers a large area of the nation's overall geographical area. It is mostly seen along the Red Sea in the Eastern Desert, with isolated examples in the Western Desert around Gebel Oweinat. The Neoproterozoic supercontinent cycle that produced the Eastern Desert as a component of the ANS was bound by the dissolution of Rodinia and the formation of Gondwana (Kroner and Stern, 2004). The Nubian Shield, which was a continuous portion of the Arabian Peninsula's Arabian Shield prior to the entrance of the Red Sea, is made up of the basement rocks of Egypt's Eastern Desert. It is widely believed that the Pan-African orogeny, which took place around 570 Ma, is what caused the Nubian Shield's basement to become cratonized (El Gaby et al., 1988). Neoproterozoic Pan-African thrusting, which is distinguished as migmatites, cleaved granites, and infrastructure gneisses that form suprastructural units, was present during this orogeny and can be found in places like Hafaft, Barramiya, and Meatiq. Aside

from that, the ANS is significant structurally and economically because it contains precious base metals such as gold, copper, zinc, silver, sulfur, chromite, and nickel (Stern, 1994; Johnson et al., 2011). Gold deposits are associated with alteration zones in Egypt's central and southern Eastern Desert such as the El-Barramiya area and Dungash area (Salem et al., 2016; Saleh et al., 2018; Mohamed et al., 2022; Abdelrady et al., 2023a,b). The central eastern desert of Egypt includes the Barramiya area, Dungash area, and other areas (Fig. 1). The region under examination is situated in the middle eastern desert of Egypt, between longitudes 33° 33′ 00″ and 34° 05′ 00″ E and latitudes 24° 49′ 00″ and 25° 16′ 00″ N. It includes different rock units such as ophiolites, serpentinite, metagabbro to metadiorite, basic, intermediate and acidic metavolcanics, metasediments, gabbroic rocks, calc-alkaline and alkaline rocks and sedimentary rocks. Deformed gabbro-diorite sliced through the ophiolitic mélange and metasediments in the research area's central regions. Furthermore, several differently foliated intrusions of older granitoids pierce the ophiolitic rocks in the study area's northwest. The primary foliation of the mélange matrix is deeply penetrated by weathered, post-tectonic granite and granodiorite. According to Johnson et al. (2011), the protolith age of these rock associations ranges from 810 to 720 Ma, reflecting Neoproterozoic period. Only the areas where the steeply sloping NW–SE and E–W faults connect, which dip steeply, are home to younger granites. There is unconformity between the sedimentary rocks that cover the research area's westernmost region and basement rocks. The area contains many features which are considered landmarks in the Eastern Desert such as the Barramiya gold mine, Dungash gold mine, Bir Dungash, Gebel Um Salatit, Gebel

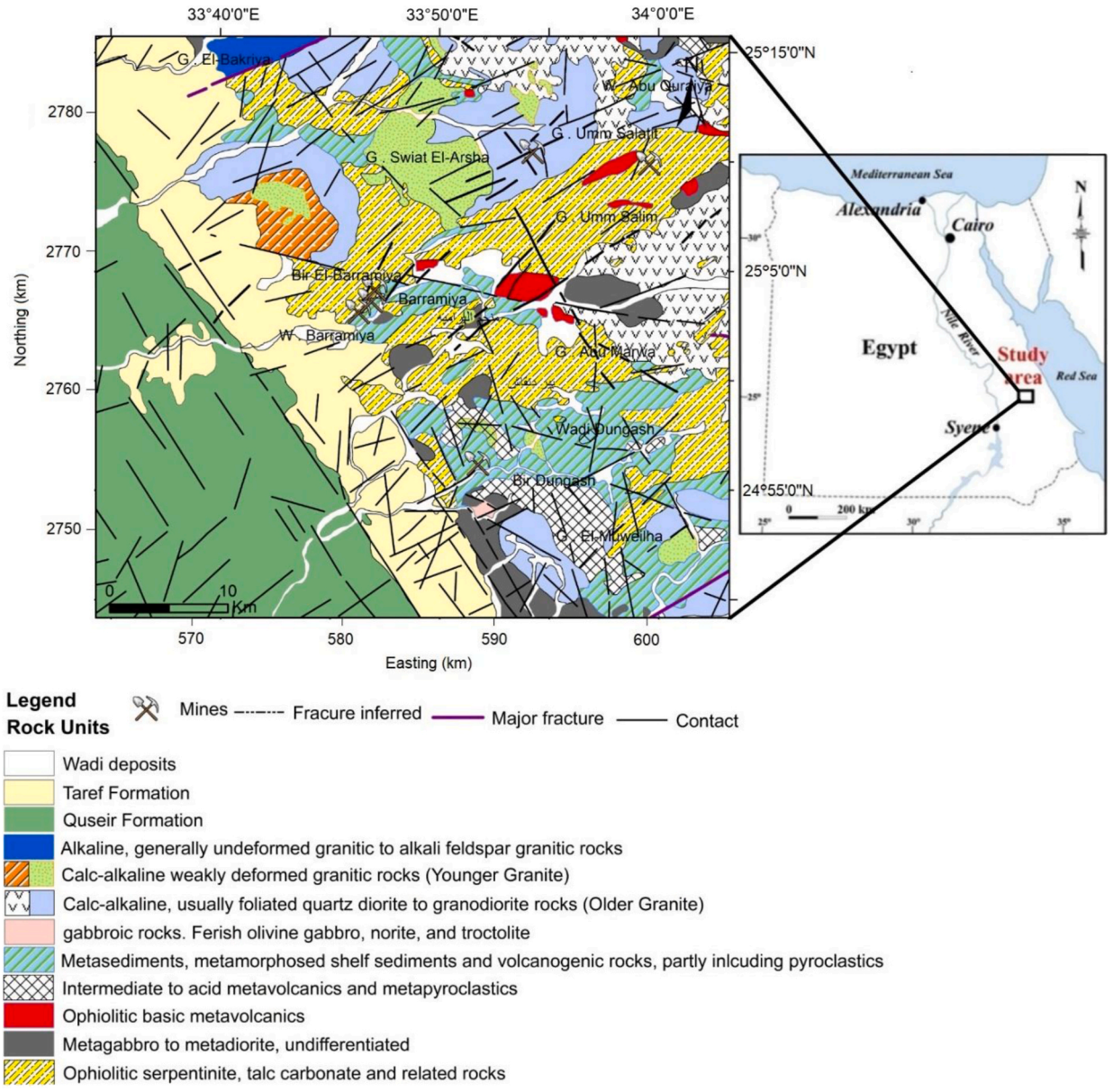


Fig. 1. Geologic map of the study area after CONOCO (1987). Inset showing a location map.

Umm Salim, and Gebel El-Mueilha. The country rocks are made up primarily of ophiolitic mélange, the serpentinite blocks and clasts that make up the mélange are allochthonous, fragmented, and jumbled together inside an actinolite and graphite schist matrix that has undergone extensive deformation. The serpentinite in the Barramiya-Mueilha area is made up of cumulus ultramafic rocks that have undergone greenschist facies metamorphosis (Ali-Bik et al., 2012; Abdelazeem et al., 2019; El-Ela et al., 1985). One of the Nubian Shield's biggest and most noticeable outcrops of serpentinites and talc-carbonate rocks is found in the Barramiya region. Serpentines, talc-carbonates, and quartz-carbonate rocks (listvenite) are examples of ophiolitic units. The island arcs metavolcanic rocks in the research region (Fig. 1) include metabasalt, basaltic meta-andesite, interbedded dacitic tuffs and agglomerate, with incidental carbonate pieces. Weakly deformed rocks called metagabbro-diorite complexes underlie a large region in Wadi Beizah. The study area's northernmost region, which is bordered by the ENE-WSW Barramiya-Um Salatit belt, is dominated by ENE-trending dikes. The infrastructure/suprastructure contact in the Eastern Desert's central region is a zone of significant strain that has been characterized as a thrust, an extensional fault, and more (Ries et al., 1983; Sturchio et al., 1983; Fritz et al., 2002). The Dungash belt has undergone several structural deformation episodes, producing folds and uplifts with NE-SW and NW-SE trending axes. These formed in the ultramafics, producing parallel sheets with a NW-SE trend that dipped to the southwest and thrust over the metavolcanics (Salem et al., 2016). The zone of mineralization stretches up to 1 km along strike and 400 m down dip, with quartz and quartz-carbonate veins ranging in width from 10 cm to 1 m in the Barramiya area. Within a strongly altered sequence of island-arc metavolcanic and metavolcaniclastic rocks and banded iron formation, the gold mineralization consists of a system of massive and sheared, milky quartz-sulfide veins that trend north-west and are hosted by an N-trending Najd fault that contains sheared serpentinite in the Abu Marawat area (Zoheir and Akawy, 2010).

3. Material and method

3.1. Material

Together with the aeromagnetic dataset, this study employed ALOS PALSAR (Advanced Land Observing Satellite Phased Array Type L-band Synthetic Aperture Radar) data to delineate structural features within the study area. A 12.5-m resolution radar dataset acquired in Fine Beam Single polarization (HH) mode was obtained from the Alaska Satellite Facility. ALOS PALSAR's L-band SAR offered all-weather, day-and-night data acquisition, enabling the generation of high-resolution digital elevation models (DEMs). This dataset was selected over other remote sensing options due to its demonstrated effectiveness in detecting structural elements (Shebl and Csámer, 2021), particularly in arid environments. L-band radar waves exhibit relatively greater penetration depth through thin covers in arid environments compared to shorter wavelengths (Shebl and Csámer, 2021). This allows for the detection of near-surface geologic interfaces and variations in subsurface material properties, enabling comparative analysis with aeromagnetic data to enhance the understanding of geological conditions.

Geological formations in a variety of tectonic settings and geographic locations may be mapped using aeromagnetic surveys. Recently, many aeromagnetic datasets covering different areas have been used in Egypt to map subsurface structures (Elkhateeb, 2021; Saada et al., 2021b; Hamimi et al., 2023). This study's aeromagnetic data came from the Egyptian Geological Survey. Making use of the IGRF values for the year 2020 (i.e., total field = 42425 nT, inclination = 32.8°, and declination = 1.9°), The Earth's magnetic field's regional impact was removed from the aeromagnetic data. The aeromagnetic dataset of the El-Barramiya-Dungash area was interpolated with a grid spacing of 100 m. The aeromagnetic map symbolizes the crust's and the lithospheric mantle layers' magnetic reactions (Melouah, 2023). The edge enhancement techniques can be applied to this dataset to outline the shallow and deep structures that control mineralization in the study region.

3.2. Textural analysis

This study employed Grey-Level Co-occurrence Matrices (GLCMs) – also known as grey-level spatial dependence matrices – for a comprehensive textural analysis (Haralick, 1979; Li, 2011; Shebl and et al., 2024). GLCMs have demonstrated efficacy across diverse datasets, including aeromagnetic and remote sensing data imagery (Ghosh, 2022; Shebl and et al., 2024), making them suitable for lithological and structural mapping. Textural attributes are derived by quantifying spatial relationships between neighboring pixels. A moving window of a specified size is applied to the image, assessing the digital values of all pixels within its confines. This approach enables the evaluation of pixel pair relationships, with the level of detail determined by the window size and the spatial resolution of the imagery. The window size, represented by the number of pixels (N) – for example, 81 pixels for a 9×9 window – influences the granularity of the analysis. This second-order statistical analysis generates a suite of textural descriptors, including mean, variance, dissimilarity, second moment, and correlation. This research, following an evaluation of various kernel sizes, employed a 15×15-pixel kernel for optimal structural delineation.

3.3. Edge enhancement techniques

Numerous filtering processes should be used for aeromagnetic data to identify the lineaments and geological structures that aid in depositing mineralizations across the El-Barramiya-Dungash area. To enhance the geological edges, we applied some filters, including MTM, TAHG, HGSTDR, FS, EHGA and BHG to upward continue magnetic datasets of the area.

3.3.1. TAHG

The TAHG method was introduced by Ferreira et al. (2013), which is given by:

$$TAHG = atan \frac{\frac{\partial HG}{\partial z}}{\sqrt{\left(\frac{\partial HG}{\partial x}\right)^2 + \left(\frac{\partial HG}{\partial y}\right)^2}}, \tag{1}$$

where $\frac{\partial HG}{\partial x}$, $\frac{\partial HG}{\partial y}$ and $\frac{\partial HG}{\partial z}$ are the gradients of the HG of the field F, which is determined by:

$$HG = \sqrt{\left(\frac{\partial F}{\partial x}\right)^2 + \left(\frac{\partial F}{\partial y}\right)^2}. \tag{2}$$

The TAHG transform range is between -π/2 and +π2, which is due to the properties of the arctangent. Since TAHG is a normalized method, it can balance signals coming from both shallow and deep structures. TAHG provides maximum amplitudes over the source boundaries, and it can avoid producing false information in the output maps, making it helpful to delineate the geological structures.

3.3.2. MTM

Although the edges defined using the TM technique (Wijns et al., 2005), which equalizes HG by TG, are balanced, these edges are diffuse. Its improved approach (MTM) is described by, which uses high-order gradients of the field:

$$MTM = acos \frac{\sqrt{\left(\frac{\partial^2 F}{\partial z \partial x}\right)^2 + \left(\frac{\partial^2 F}{\partial z \partial y}\right)^2}}{\left(\frac{\partial^2 F}{\partial z \partial x}\right)^2 + \left(\frac{\partial^2 F}{\partial z \partial y}\right)^2 + \left(\frac{\partial F}{\partial z} \Big/ (p \times h)\right)^2}, \tag{3}$$

where h is the sample step, and p is a number ranging from 0.05 to 5. The MTM uses minimum values to outline the edges. Since this method uses second gradients, it is sensitive to noise. However, the MTM results have a very high resolution, providing clear edges for geological bodies.

3.3.3. HGSTDR

Nasuti et al. (2019) introduced HGSTDR to recognize the edge of anomalies. The method is given by:

$$HGSTDR = \sqrt{\left(\frac{\partial STDR}{\partial x}\right)^2 + \left(\frac{\partial STDR}{\partial y}\right)^2}, \tag{4}$$

where STDR is the second tilt derivative, and is defined as:

$$STDR = \text{atan} \frac{M \times \frac{\partial^2 F}{\partial z^2}}{\sqrt{\left(\frac{\partial HG}{\partial x}\right)^2 + \left(\frac{\partial HG}{\partial y}\right)^2}}, \tag{5}$$

with $\frac{\partial^2 F}{\partial z^2}$ is the second vertical gradient of the field. The HGSTDR filter provides the highest values over the borders of anomalies. The HGSTDR filter employs third vertical derivatives, which might lead to noisy results. The use of the HGSTDR filter brings the sharpest signals over the edges compared to other filters, therefore, it is effective in mapping a wide range of geological features.

3.3.4. FS

The fast sigmoid detector (FS) was recently developed by Oksum et al. (2021). The filter produces a clear view of the source's edges, and is given by

$$FS = \frac{R - 1}{1 + |R|}, \tag{6}$$

where

$$R = \frac{\frac{\partial HG}{\partial z}}{\sqrt{\left(\frac{\partial HG}{\partial x}\right)^2 + \left(\frac{\partial HG}{\partial y}\right)^2}}. \tag{7}$$

Maximum amplitudes of the FS filter are used to identify anomalous sources' edges. Since the FS makes use of the ratio of derivatives of HG, it can balance signals coming from both shallow and deep structures. In addition, the FS filter does not yield false edges. For these reasons, the FS filter efficiently maps a broad variety of geological structures.

3.3.5. EHGA

Pham et al. (2022a) suggested the EHGA filter based on GA's derivatives to map the edges. The EHGA filter can be specified as follows:

$$EHGA = \mathscr{R}\left(\operatorname{asin}\left(k\left(\frac{\frac{\partial HG}{\partial z}}{\sqrt{\left(\frac{\partial HG}{\partial x}\right)^2+\left(\frac{\partial HG}{\partial y}\right)^2+\left(\frac{\partial HG}{\partial z}\right)^2}}-1\right)+1\right)\right), \tag{8}$$

where k is a positive constant selected by the interpreter ($k \geq 2$), and $\mathscr{R}$ is the real part. Due to the arcsine function's characteristics, EHGA ranges from $-\pi/2$ to $+\pi/2$. It is a normalization of the vertical derivative of the HG; therefore, it can simultaneously identify both shallow and deep structures. Maximum amplitudes in the EHGA map are used to identify the borders. The EHGA method permits better detection of the geological edges, as well as better highlighting some structures that either are not depicted in the HG technique and other techniques or not very well mapped.

3.3.6. BHG

The BHG filter is a different balancing method that also maps the edges of sources using maximum values. This approach is given by (Prasad et al., 2022):

$$BHG = atan\left(\frac{(k-1)\frac{\partial HG}{\partial z}-(k+1)\times\sqrt{\left(\frac{\partial HG}{\partial x}\right)^2+\left(\frac{\partial HG}{\partial y}\right)^2}}{\left|(k-1)\frac{\partial HG}{\partial z}-(k+1)\times\sqrt{\left(\frac{\partial HG}{\partial x}\right)^2+\left(\frac{\partial HG}{\partial y}\right)^2}\right|}\right), \tag{9}$$

The BHG filter can balance anomalies with different amplitudes, and generates maximum values over the source boundaries. Like the TAHG, FS, and EHGA filters, the BHG filter not only avoids bringing false edges but also yields geological boundaries with greater resolution than other techniques.

3.4. Upward continuation

The upward continuation approach helps to reduce or eliminate the impact of noisy and shallow sources to enhance the signal from deeper bodies in the survey region. By computing data collected at elevations greater than those observed in the field, the magnetic anomalies at various heights farther from the causal source are recovered (Jacobsen, 1987). Potential field conversion from a flat plane

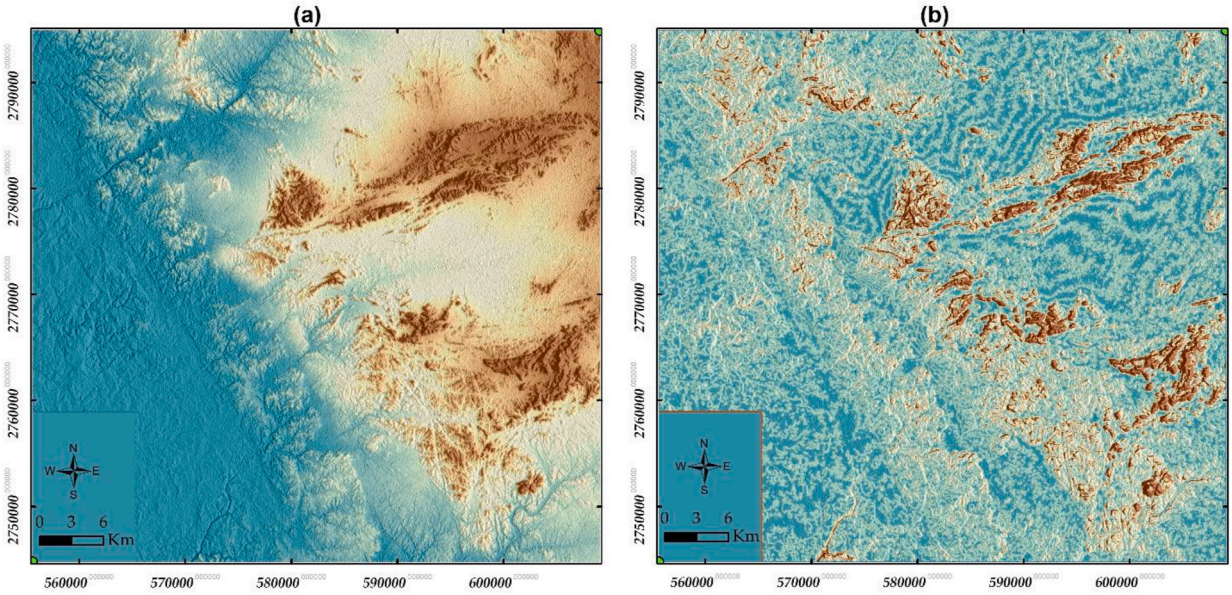


Fig. 2. (a) Spatial distribution of mean values derived from ALOS PALSAR data, effectively distinguishing sedimentary rocks in the west from basement rocks (east), with a prominent ENE-trending orientation of ophiolitic rocks (brown). (b) Variance map highlighting major tectonic trends (e.g., NW-SE and NE-SW) within the study area.

to a higher plane is known as an upward continuation filter (Bohal et al., 2020). Enhancing large-scale features in the survey region can be done by this filter. Some authors applied the edge detection filters to upward continued data to provide structural features more clearly (e.g., McGrath et al., 1991a, b; Ferreira et al., 2013; Nasuti and Nasuti, 2018; Sehsah et al., 2019; Abd El Wahed et al., 2025).

3.5. EUL

EUL is a semi-automatic technique that is widely used as a tool for deciphering potential data (Reid et al., 1990; Pham et al., 2024). It automatically determines the source location (x_o, y_o, zo) using the 3D Euler's equation (Reid et al., 1990):

$$(x-xo)\frac{\partial F}{\partial x}+(y-yo)\frac{\partial F}{\partial x}+(z-zo)\frac{\partial F}{\partial x}=N(B-F), \tag{10}$$

where B is the regional value of the field, and N represents the structural index (SI), which has values between zero and three depending on the shape of the source body. For example, N = 0 is used for detecting contacts, N = 1 for thin sheets like dike and sill, N = 2 for line sources (pipelines), and N = 3 for spheres or compact bodies.

Although remote sensing data is effective for mapping surface structures, magnetic data offers insights into deeper geological features. An integrated approach provides a powerful framework for delineating structural elements in the study area, yielding more accurate and trustworthy results and contributing to structural understanding.

4. Results

Textural analysis was applied to the ALOS PALSAR data to highlight the main trends within the study area. Fig. 2a shows the spatial distribution of mean values derived from ALOS PALSAR data. This map clearly separates the study area into two sectors: the eastern part, characterized by rigid terrain (brown), and the western part (blue), which is mostly flat and represents sedimentary rocks. The boundary between them is marked by a NW-trending unconformity surface, as depicted in Fig. 2a by the contrast between the two colors. Nearly perpendicular to these NW-trending structural elements, several NE-SW-trending structural features are represented by structurally controlled wadis. Furthermore, a clear manifestation of these NE-SW trends is observed in the lithological orientation (ENE-WSW) of the ophiolitic rocks of Gabal Um Salim and Gabal Um Salatit, which are part of the well-known Baramiya-Mubarak shear zone. This zone exhibits dextral displacement in the ENE–WSW direction, as stated by Shebl, 2023. Fig. 2b illustrates the variance values, clearly depicting these tectonic trends. The higher variance values (brown) highlight deformed ophiolitic blocks primarily trending NE-SW, and the mutation of lines (created from the contrast between low and moderate values) around these blocks further confirm the orientation, while also highlighting transpressional and transtensional shear zones within the study area. Additionally, close examination of these lines reveals the dominant trends and forms of the main lithologies within the study area, particularly around Gabal Barramiya and Gabal Um Salatit. To the south of Gabal Um Salatit, a consecutive folding pattern is observed, which has been documented through remote sensing and field observations in previous studies.

To better understand and emphasize these differences, more specific textural elements were utilized, including second moment and

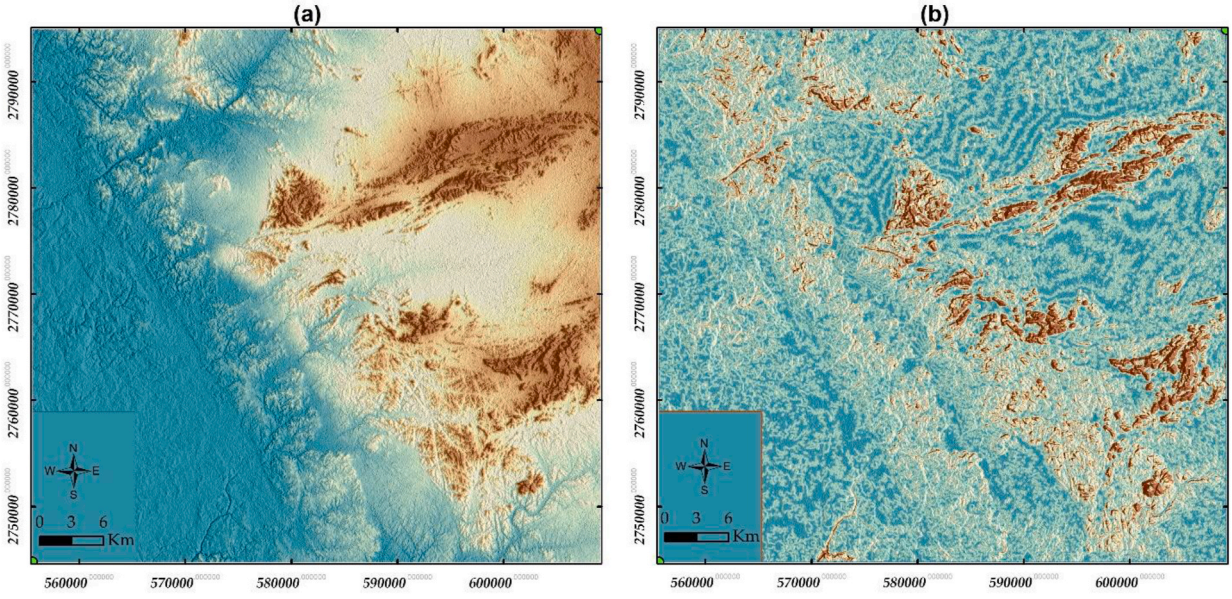


Fig. 3. Textural Analysis Maps. (a) Second Moment map, (b) Dissimilarity map, highlighting lithological variations and emphasizing structural trends, including the ENE-trending ophiolite belt.

dissimilarity as statistical measures that capture different aspects of the texture of the studied terrain, as displayed in Fig. 3. In Fig. 3a, the low second moment and high dissimilarity of ophiolitic rocks reflect their highly heterogeneous and structurally complex nature, distinguishing it from other lithologies. These findings enhance our understanding of textural variations in geological formations and their implications for detailed structural analysis. The low second moment in ophiolitic serpentinite indicates a highly heterogeneous texture resulting from serpentinization, which introduces mineralogical and structural variation. The mix of serpentine, magnetite and talc creates a non-uniform pattern with high pixel intensity disorder, further amplified by veins, fractures, and tectonic shearing. Similarly, the lower second moment in metavolcanics and mélange matrix also reflects their complex textural characteristics. In the southwestern part of the study area, sedimentary rocks (e.g., the Tarif formation) exhibit higher second moment values due to their uniform grain size, layered structure, and lower mineralogical contrast compared to igneous and metamorphic rocks. Their well-sorted composition, minimal deformation, and compacted texture result in a more consistent pattern with less intensity variation, leading to higher second moment values than those found in more heterogeneous and structurally complex rocks like serpentinite. In contrast, igneous and metamorphic rocks in the eastern part of the study area display higher dissimilarity (Fig. 3b) than the sedimentary rocks in the west, owing to their greater mineral diversity, structural deformation, and complex textures. Sharp mineral contrasts, fractures, and foliation generate strong intensity variations, while sedimentary rocks show more uniform transitions. This underscores the dynamic geological processes and deformation-driven heterogeneity of the basement rocks.

To better highlight these deformations, correlation was applied to the study area, as it is useful for detecting linear elements, which often align in specific directions. By analyzing the orientation and distribution of texture features, correlation helps identify patterns that reveal linear geological structures (Fig. 4). A general overview of Fig. 4 indicates the highest correlation and orientations within igneous and metamorphic rocks, compared to sedimentary rocks. A closer view is presented in Fig. 5 to emphasize the main structural trends identified through the ALOS PALSAR data. For example, Fig. 5a clearly depicts NW-SE trending rocks. Fig. 5b illustrates subhorizontal structures swinging along E-W trends, which is confirmed in the upper part of Fig. 5c. The latter also clearly shows NE-

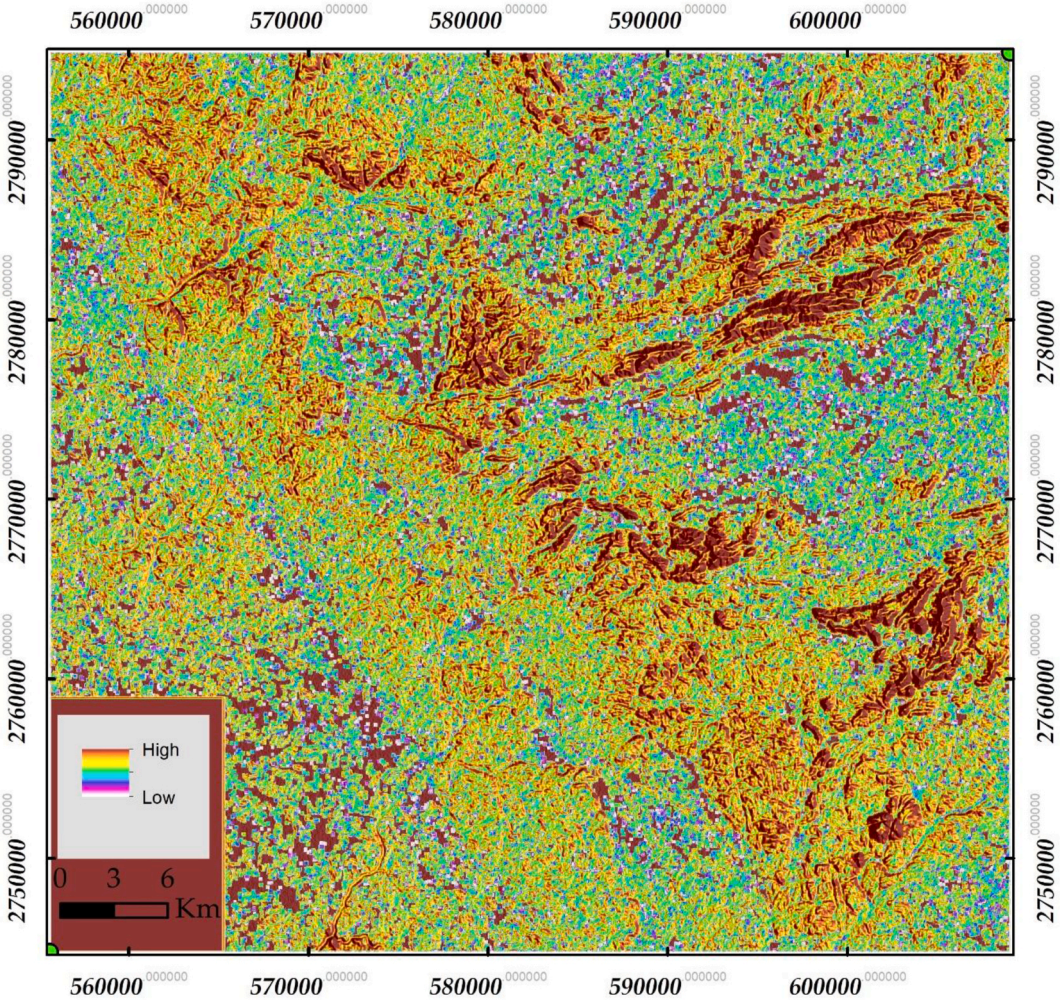
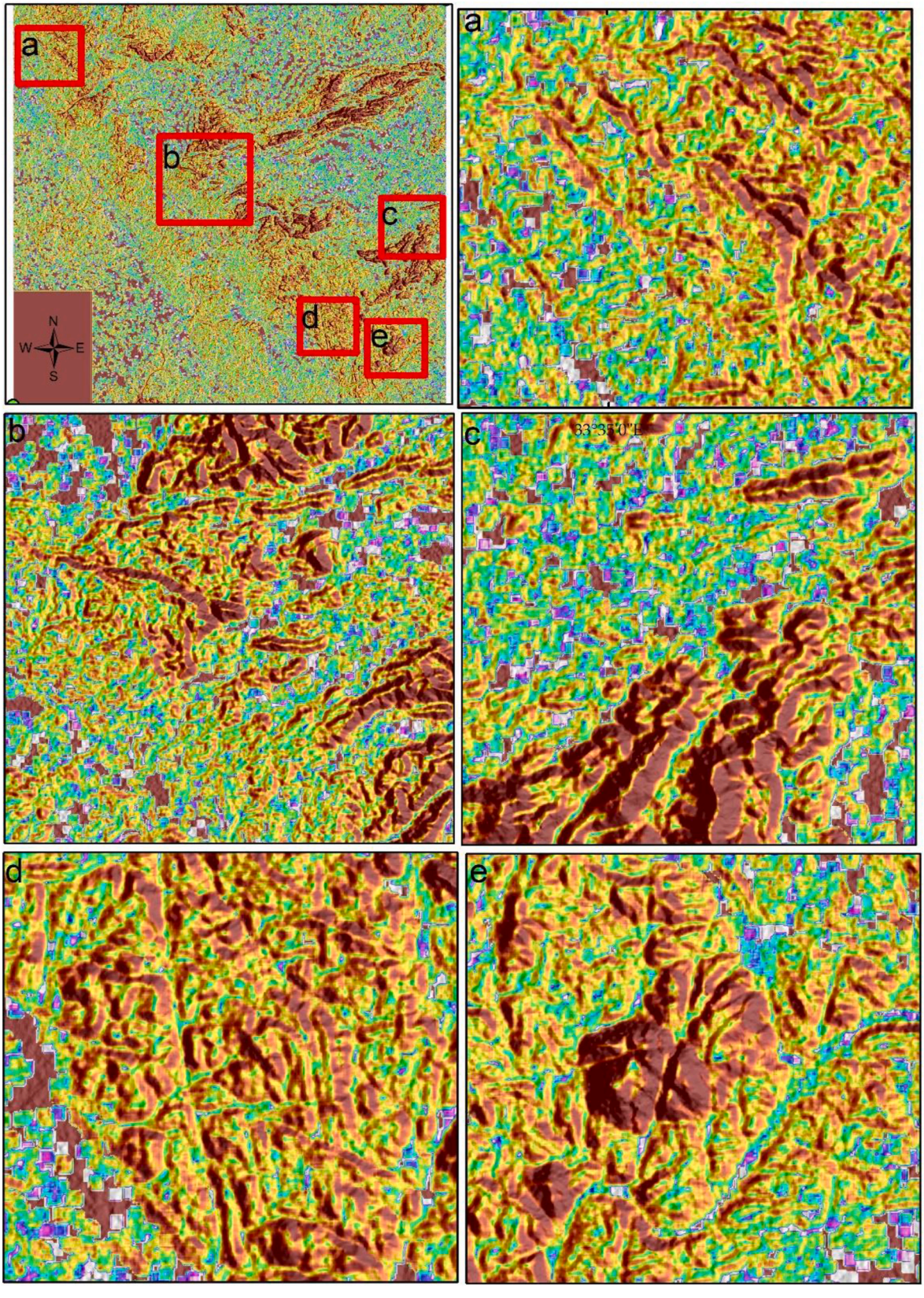


Fig. 4. Pseudo-color map illustrating spatial variations in correlation values. Linearly dependent pixel pairs exhibit higher correlation values, effectively highlighting potential lineaments within the exposed rock units.



(caption on next page)

Fig. 5. Close-up views of the correlation map (Fig. 4) highlighting prominent structural trends: (a) NW-SE, (b) subhorizontal trending approximately E-W, (c) E-W and NE-SW, (d) subvertical N-S, and (e) cross-cutting NW and NE structures, consistent with aeromagnetic data interpretations.

trending rocks. Fig. 5d reveals an almost vertical N-S trend, along with NE-SW trends that intersect in a cross-cutting relationship. This cross-cutting relationship is further depicted in Fig. 5e, where the trend is cut and displaced in a sinistral sense by a NE-trending fault.

In addition to remote sensing data, we also used magnetic data to map geological structures in the El-Barramiya-Dungash area. The magnetic field of the area is examined prior to using the improved enhancement approaches. Fig. 6a shows the aeromagnetic map of the area. The aeromagnetic dataset in the research area varies from −1180 to 2854 nT with an average value of 1524 nT. Fig. 6b depicts the RTP aeromagnetic map calculated for the research region with an inclination of 32.8° and a declination of 1.9°. The NE-SW, NW-SE, and N-S anomaly patterns predominate in the RTP data, which range from −951 to 3357 nT. The RTP's magnetic signature displays anomalies with a variety of amplitudes and wavelengths, signifying the various magnetic structures. The positive anomalies in the research region are related to serpentinite rocks, ophiolitic basic metavolcanic rocks, gabbroic rocks, and metagabbro that have higher content of Iron-minerals leading to high magnetic susceptibility. The negative magnetic anomalies are related to Wadi deposits and other sedimentary rocks, metasediments, and felsic rocks including alkaline and Calk-alkaline rocks.

It is preferable to use a low pass filter to reduce the noise level before using approaches based on derivatives of aeromagnetic data since genuine aeromagnetic data often contains noise. RTP aeromagnetic data may be subjected to an upward continuation filter to address this problem. Here, we applied a 200 m upward continuation filter to the RTP aeromagnetic data of the region. The upward-continued data is shown in Fig. 7a. Findings from applying the MTM, TAHG, FS, EHGA, HGSTDR, and BHG techniques to data in Fig. 7a are shown in Fig. 8a–f, respectively. The magnetic boundaries identified using these approaches show a high correlation. By comparing these maps, we can see that the TAHG, EHGA, FS, and BHG techniques provide similar results. However, the EHGA and FS create sharper signals over the boundaries than TAHG. MTM and HGSTDR show the borders with very high resolution, but the edges are connected, making it challenging to identify actual geological features.

To further decrease the noise impact, a 1000m upward continuation was applied to the RTP aeromagnetic data. Fig. 7b displays upward-continued RTP aeromagnetic data. By comparing these maps, we can notice that the final data is smoother than the 200 m upward continuous one, but the basic magnetic field structures are still there (Figs. 6b, 7a and 7b). The findings from applying the TAHG, MTM, HGSTDR, FS, EHGA, and BHG techniques to 1000 m upward-continued RTP data in Fig. 7b are shown in Fig. 9a–f, respectively. Again, the boundaries determined by the MTM and HGSTDR maps are connected, leading to wrong structural interpretations. In addition, as reported by Eldosouky et al. (2022b) and Ai et al. (2024), the MTM and HGSTDR tend to produce false edges. We can see that the EHGA, FS, and BHG are still the best maps to detect geological structures compared with other methods.

The RTP aeromagnetic data was subjected to additional analysis using the EUL method to more accurately describe the underlying geological features and determine their depth. The result of the EUL technique is shown in Fig. 10. We can see that the majority of subsurface structures have depths between 159 and 920 m, with an average depth of 382 m. These findings indicate that the NW-SE, NE-SW, and E-W are major trends in the El-Barramiya-Dungash region.

5. Discussion

The textural analysis of the ALOS PALSAR data provides a detailed visualization of the multi-phase deformation history of the study area, consistent with previous structural models (Shebl and et al., 2024; Shebl and Csámer, 2021; Zoheir, 2019). The NE-SW and NW-SE trending structural features identified through variance and textural correlation directly correspond to the D1 and D2 deformation phases, respectively, as documented by Shebl and Csámer (2021) and Zoheir, 2019. The D1 phase, resulting from NNW-SSE shortening, is responsible for the prominent NE-SW trends observed in deformed ophiolitic blocks and the dextral Baramiya-Mubarak shear zone. Conversely, the D2 phase, caused by NNE-SSW shortening, manifests as the significant NW-SE trending features that define the major lithological boundaries. The low second moment and high dissimilarity values observed in the ophiolitic rocks and mélange matrix serve as a direct textural expression of the intense shearing and structural complexity associated with these two main deformation events. Furthermore, the detailed analysis of textural correlation and orientation highlights the combined and superimposed effects of these deformation phases. The sub-horizontal trends (ENE-WSW to WNW-ESE), which are a clear feature in the study area, are a direct consequence of the collective influence of the D1 and D2 phases. The presence sub-vertical N-S trending features, particularly where they cross-cut and displace older trends in a sinistral sense, perfectly aligns with the later D3 phase, characterized by E-W oblique convergence (Zoheir, 2019). Thus, ALOS PALSAR textural analysis supports the multi-phase structural framework and clearly maps complex structural features, especially when integrated with other data like aeromagnetic maps.

No individual technique stands out as the optimal tool for determining geological boundaries; an integrated approach consistently yields superior correlation and evaluation, providing more precise information in the study area. The findings show that the MTM, TAHG, HGSTDR, EHGA, FS, and BHG are capable of balancing anomalies with various amplitudes. This is because the foundation of these techniques is the ratio of derivatives of the field. This balancing impact is helpful in the research region where the magnetic map is characterized by high amplitude anomalies with the NE-SW, NW-SE, E-W, and N-S trends dominating the magnetic map. The results from the MTM, TAHG, HGSTDR FS, EHGA, and BHG analyses, are highly correlated with one another. The lineament analysis is an effective technique for providing information on the primary fracturing and faulting tendencies from which we may infer the prior forces that may have affected the region. A crucial element of potential fieldwork that would enable us to quickly talk about subsurface tectonic trend analysis. The lineaments are traced using the EHGA, FS, and BHG maps of 200 m and 1000 m upward-continued RTP data are illustrated in Fig. 11 a and 11 b, and the lineaments of the 200 m upward continuation are superimposed on 1000 m upward

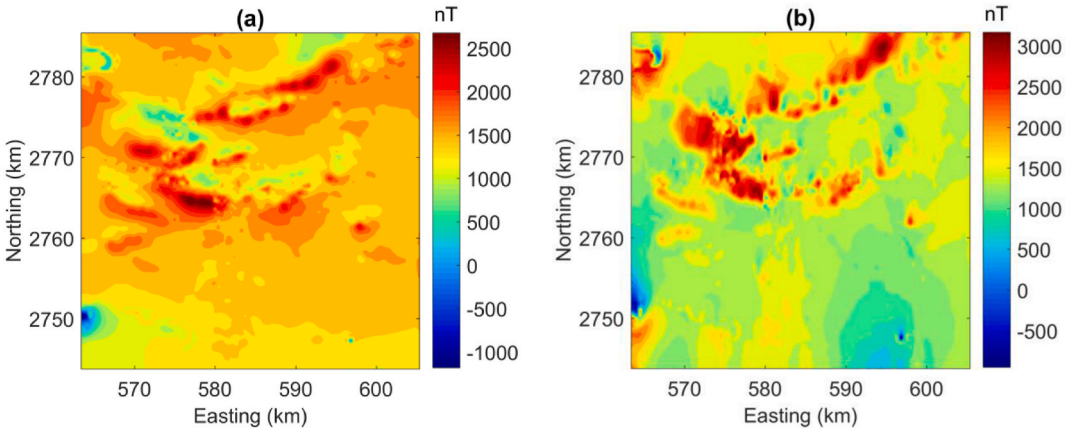


Fig. 6. Aeromagnetic map (a) and RTP aeromagnetic map (b) of the study area.

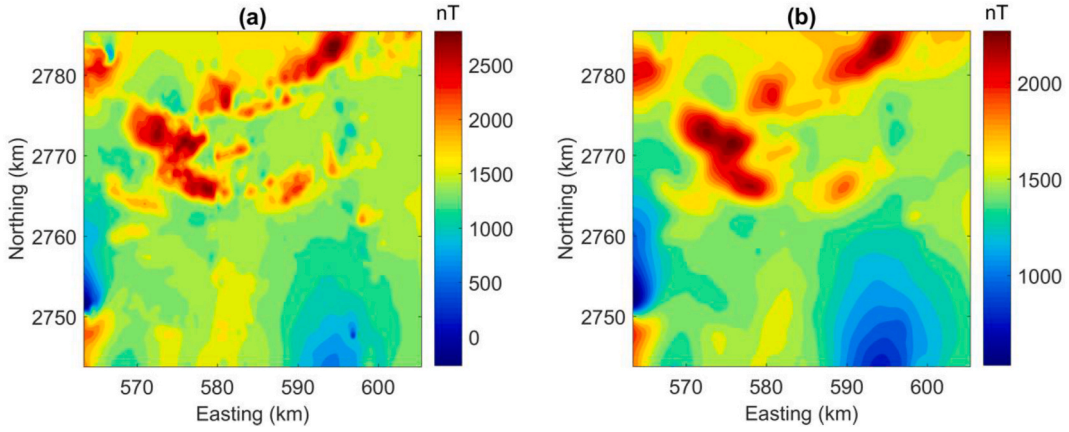


Fig. 7. (a) 200 m upward continued RTP data, (b) 1000 m upward continued RTP data.

continuation (Fig. 11e). It is clear that the magnetic lineaments of the 200 m upward continued data and the 1000 m upward continued data strongly correlate with one another and exhibit a substantial association. These figures show that the predicted magnetic boundaries agree with MTM, HGSTDR and TAHG maps. The main tectonic trends affecting the research area as illustrated by rose diagrams in Fig. 11c and d are NNE-SSW, NE-SW, NW-SE, N-S and E-W which seemed to be concordant with the primary trends being tracked from the previous geological and geophysical studies (Salem et al., 2014; Salem et al., 2016; Saleh et al., 2018; Mohamed et al., 2022; Abdelrady et al., 2023a,b). The results of aeromagnetic data align with remote sensing investigations using ALOS PALSAR data, aiding in the resolution of the tectonic setting of the studied terrain.

The acquired findings demonstrate the value of the enhancement techniques for interpreting magnetic fields. The eastern desert's basement was divided by Greiling et al. (1994), into different structural zones based on their structural grain. These domains include the NW-SE, E-W, and N-S domains. To analyze the trends revealed by the enhancement techniques, we begin with the NNE-SSW orientation, as identified by Shukri and Lotfi (1955). This trend is marked by left-lateral strike-slip faults at the Barramiya mine site, where the presence of horizontal slickensides provides clear evidence of fault movement. This structural trend is associated with tectonic activity linked to the Gulf of Aqaba. The thrust faults that divide the ophiolitic rocks and island arc rock units trend NE-SW and NEE-SWW and dip NW. Previous scholars such as Shukri and Lotfi (1955) and Abdel Khalek (1979) took this flaw into consideration. The footwall is represented by the island arc, and the hanging wall by the ophiolitic rocks. The mylonitic foliation in the thrust zones is quite robust. The NE-SW trend, based on Egypt's tectonic framework, is associated with the Gulf of Aqaba. Moving on to the NW-SE trend, which has the same trend of the Najd fault system's sinistral shear zones. This trend is concordant with the previous work of different researchers (Abdel Khalek, 1979). According to Abdel Khalek (1979), the NW-SE trend represents lateral strike-slip fault that displaces the serpentinite range of Umm Salim and Umm Salatit. Additionally, there are two perpendicular lineation tendencies, NE-SW and NW-SE, according to Abu El-Leil and Mussa (1984). The E-W faults in Egypt began in the late Pre-Cambrian and have been occasionally active ever since, according to Klitzsch (1986) and Schandelmeier et al. (1987). Said (1962) referred to the N-S trend as the "East African trend" and thought it to be the permanent direction of faulting and dike intrusion in Egypt. Early Quaternary and Late Tertiary periods actively regenerated the N-S trend, which may have originated in the Precambrian. EL-Gaby et al. (1988)

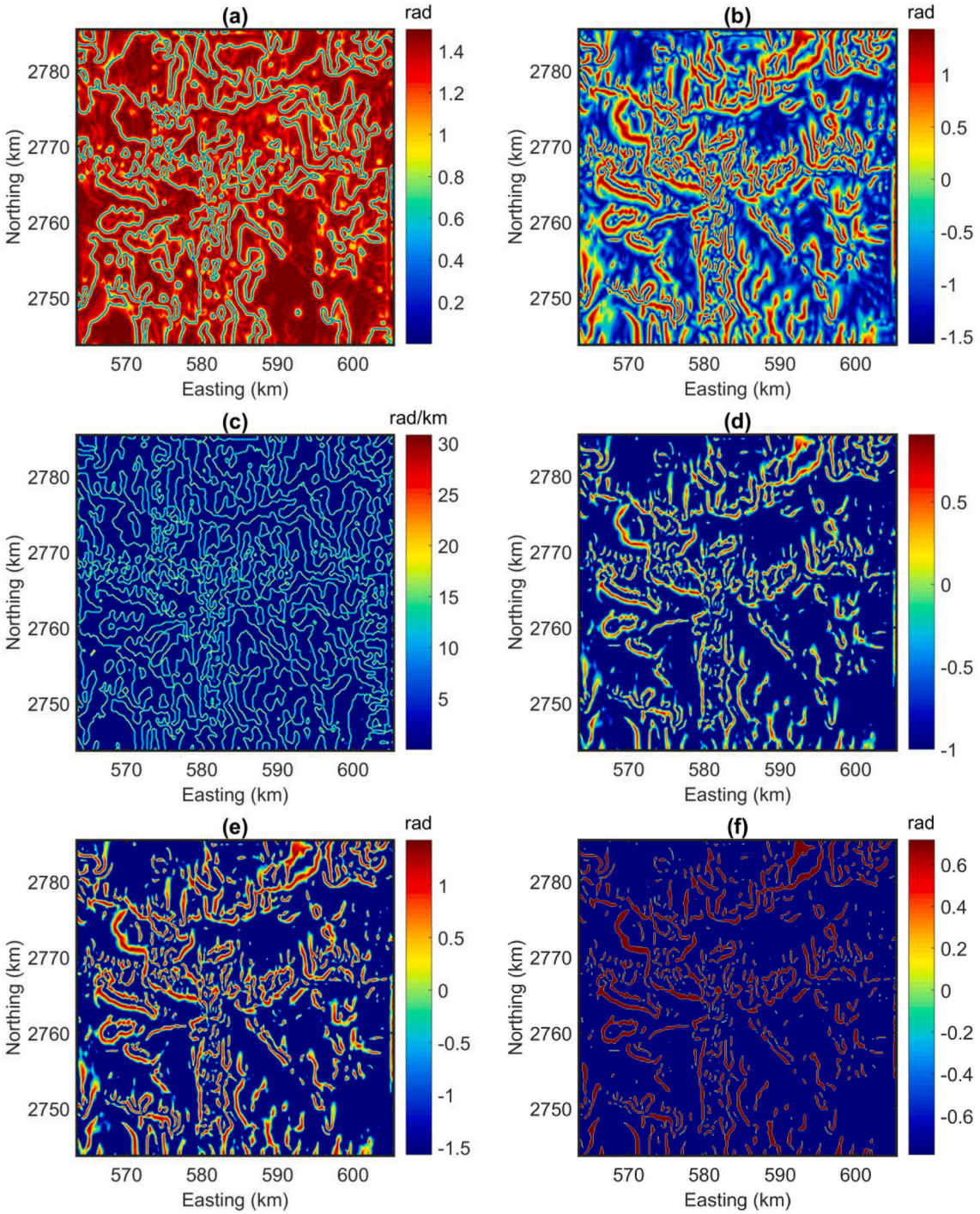


Fig. 8. Enhanced maps of 200 m upward continued RTP data: (a) MTM, (b) TAHG, (c) HGSTDR, (d) FS, (e) EHGA, (f) BHG.

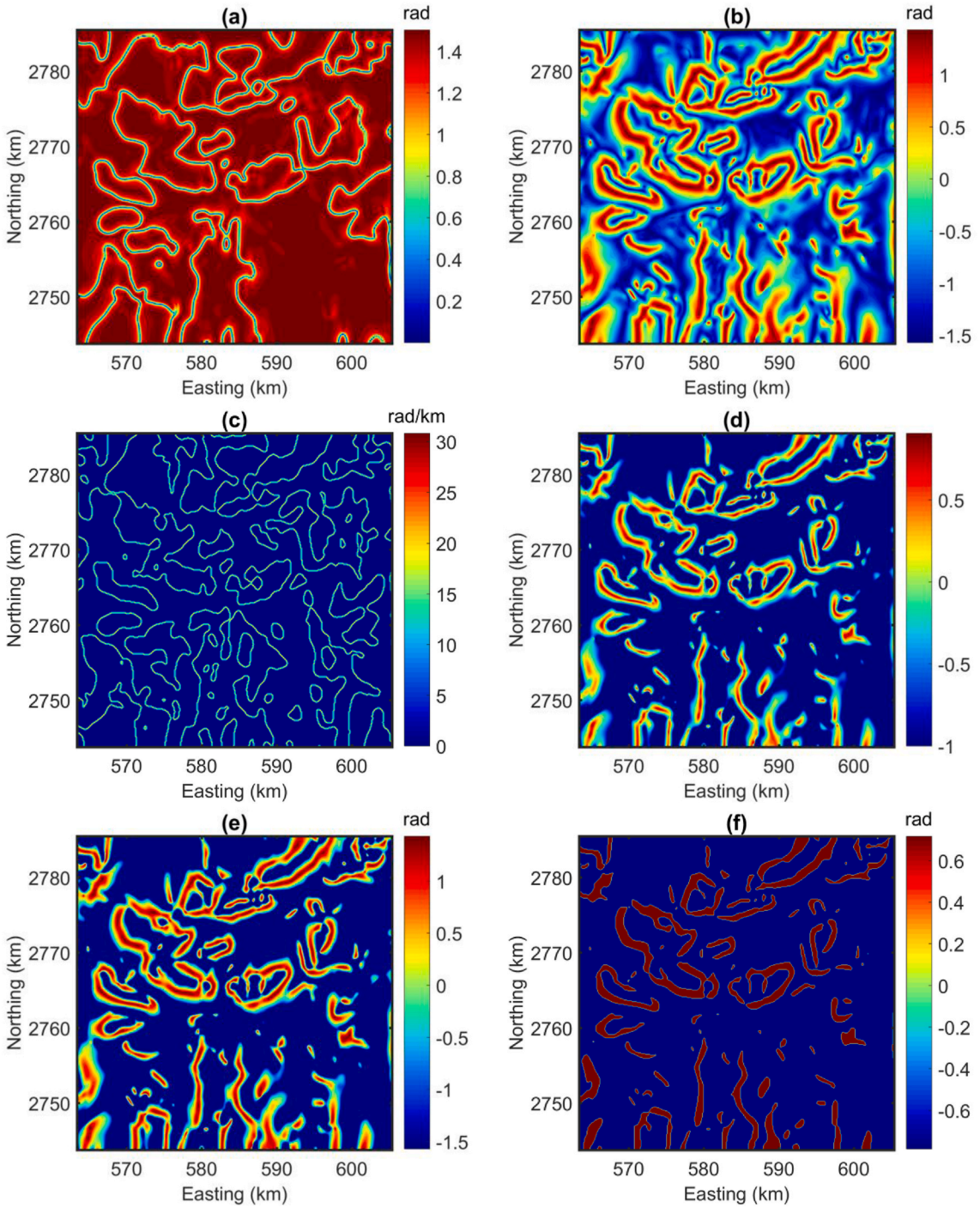


Fig. 9. Enhanced maps of 1000 m upward continued RTP data: (a) MTM, (b) TAHG, (c) HGSTDR, (d) FS, (e) EHGA, (f) BHG.

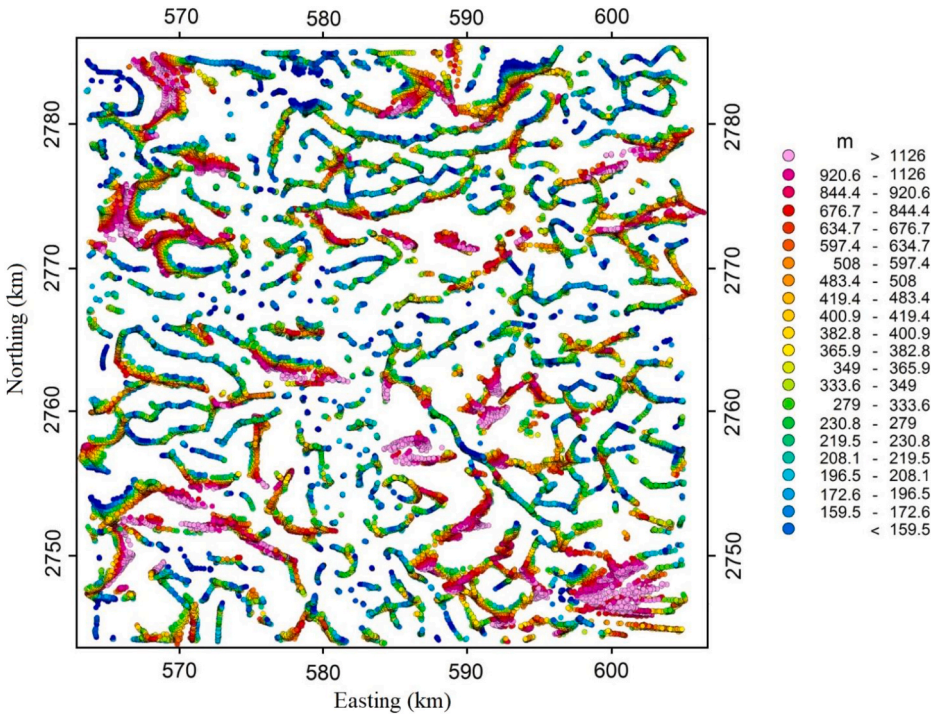


Fig. 10. The depth of the magnetic sources acquired using the EUL technique with structural index of 0.

hypothesized that the northern migration of Arabia at a greater pace than that of Africa brought about the reactivation of ancient faults by pair shearing. This trend, according to Colemen (1992), is one of Egypt's older tectonic tendencies and it is connected to the Pan-African orogeny. According to Meshref (1990), Egypt's basement rock has inherited examples of the Nubian trend.

Saleh et al. (2018) mapped the structural features of the Barramiya area using magnetic and gravity data, but their investigation only provided a few lineaments in the Barramiya area. Mohamed et al. (2022) applied the first vertical derivative, HG, TG and TA filters to magnetic data to map edges in the northern part of the study area. However, as reported by Oksum et al. (2021), Prasad et al. (2022) and Eldosouky et al. (2022b, c), the HG and TG filters are dominated by shallow sources, while the first vertical derivative and TA filters tend to generate false edges. For this reason, some lineaments detected by Mohamed et al. (2022) do not match the lineaments extracted from our interpretation (Fig. 11) using the TAHG, EHGA, FS and BHG filters that can map all the edges without false information. The structural map (Fig. 11e) established in this study is in agreement with lineaments outlined by Abdelrady et al. (2024) using the THGED filter. However, their study only provided the lineaments for a small area located in the northern part of the El-Barramiya-Dungash area. As may be seen in the structural map (Fig. 11e), a wide range of magnetic lineaments were found by using the edge filters. However, many of these lineaments are not shown in the geology map (Fig. 1) and their existence can only be inferred through magnetic interpretation. This outcome shows how beneficial the enhancement techniques TAHG, EHGA, FS and BHG are for interpreting aeromagnetic data from the El-Barramiya-Dungash area. In addition, the lineaments obtained from this study can be helpful for further studies on groundwater potential since they serve as channels or conduits for the accumulation and movement of groundwater (Ishola et al., 2023).

6. Conclusion

In the current study, recent techniques including TAHG, MTM, FS, HGSTDR, EHGA, BHG and EUL have been employed to interpret the upward continued aeromagnetic data of the El-Barramiya-Dungash region. The determined edges in the FS, EHGA and BHG maps are more obvious compared to edges found using other approaches. New information about the magnetic structures in the El-Barramiya-Dungash area is also revealed. The depth of these structures ranges between 159 m and 920 m. The results seem to be a nice tool to distinguish the terranes in the area of research. The outcomes indicate that there are a few patterns in the data, with the NNE-SSW, NW-SE, NE-SW, N-S and E-W tendencies predominating and significantly affecting the region's structural framework. These structures govern and regulate mineralization in the research region. The results from applying the enhancement filters to the aeromagnetic data of the El-Barramiya-Dungash area correspond with the major geological features in the region. Furthermore, textural analysis of ALOS PALSAR data provided valuable insights into the region's structural fabric. The analysis effectively differentiated lithological units, highlighting prominent structural trends, including the ENE-trending ophiolite belt. In addition, the analysis effectively delineated potential lineaments, including NW-SE, subhorizontal E-W, NE-SW, N-S, and cross-cutting NW-NE structures. These findings, consistent with aeromagnetic data interpretations, provide crucial information on the orientation of major structural

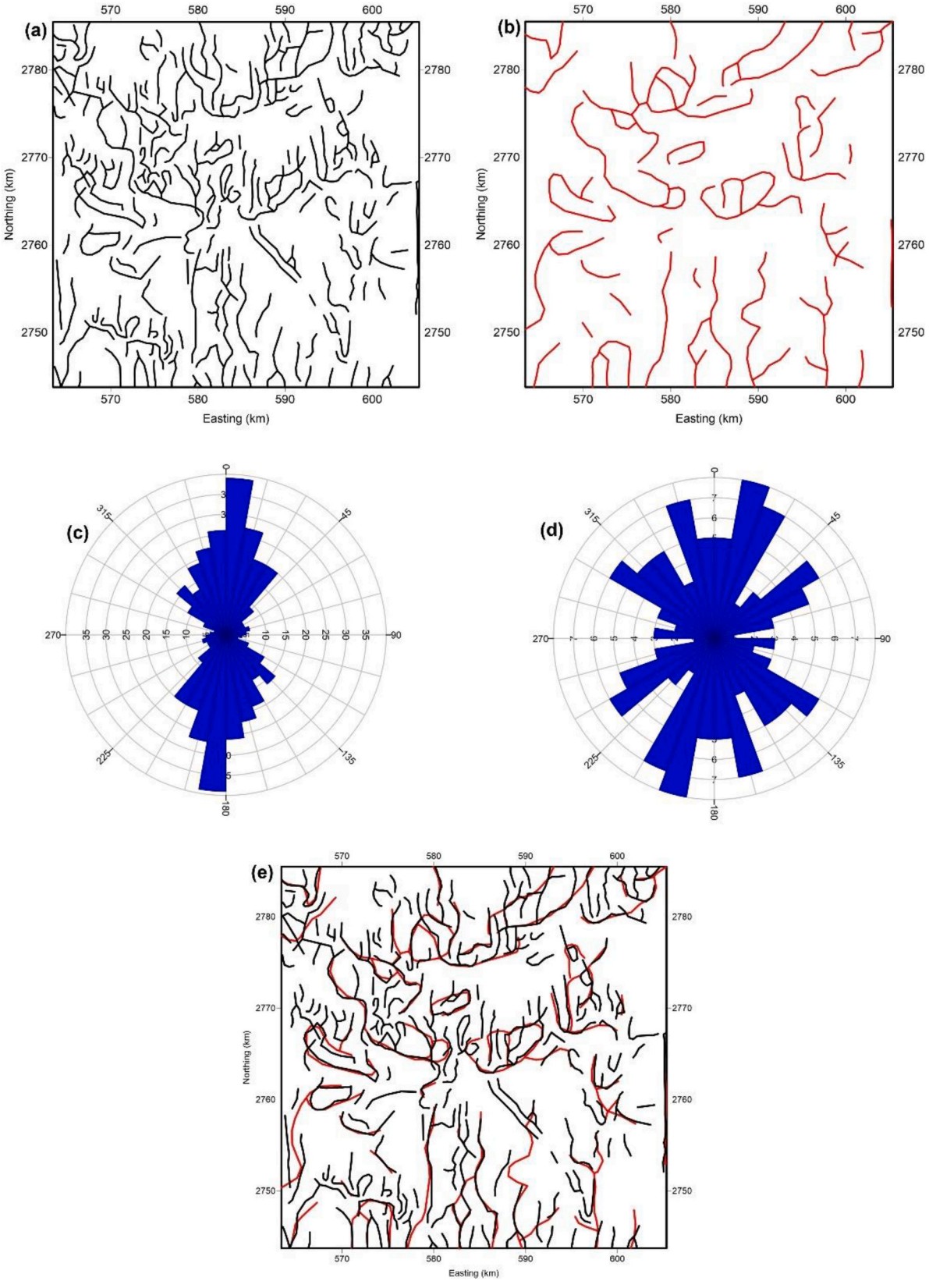

(a)
(b)
(c)
(d)
(e)
Northing (km)
Easting (km)
570
580
590
600
2750
2760
2770
2780
0
45
90
135
180
225
270
315

Fig. 11. (a) Magnetic lineaments extracted from 200 m upward-continued RTP data, (b) Magnetic lineaments extracted from 1000 m upward-continued RTP data, (c) Rose diagram of the lineaments of 200 m upward-continued RTP data, (d) Rose diagram of the lineaments of 1000 m upward-continued RTP data, (e) Structural map where lineaments from 200 m upward-continued data (black lines) are superimposed on lineaments from 1000 m upward-continued data (red lines).

features within the study area. This study demonstrates the significant potential of the integrated approach in enhancing our understanding of regional geology and can be further explored to refine structural interpretations and improve mineral exploration efforts.

CRediT authorship contribution statement

Mohamed Abdelrady: Writing – review & editing, Writing – original draft, Software, Methodology, Investigation, Formal analysis, Data curation. **Luan Thanh Pham:** Writing – review & editing, Writing – original draft, Methodology, Formal analysis. **Ferenc Molnár:** Writing – review & editing, Supervision. **Ali Shebl:** Writing – review & editing, Writing – original draft, Methodology.

Ethical statement

This article has not been previously published and is not under consideration in any other journal.

Funding declaration

No funding was received for this research.

Declaration of competing interest

The authors declare that they have no known competing financial interests or personal relationships that could have appeared to influence the work reported in this paper.

Data availability

Data will be made available on request.

References

Abd El-Wahed, M.A., et al., 2025. Structural geometry and gold ores along the first outlined N–S dextral shear zone in the Egyptian Nubian shield, East African orogenic belt: new insights from integrated remote sensing, gravity, magnetic and field studies. Geomech. Geophys. Geo-energ. Geo-Resour. 11, 76.
Abdelazeem, M., et al., 2019. A complete model parameter optimization from self-potential data using Whale algorithm. J. Appl. Geophys. 170, 103825.
Abdelkader, M.A., et al., 2024. Advanced exploration of rare metal mineralization through integrated remote sensing and geophysical analysis of structurally-controlled hydrothermal alterations. J. Geochem. Explor. 267, 107598. https://doi.org/10.1016/j.gexplo.2024.107598.
Abdelrady, M.M., 2021. Geological and Geophysical Studies of El-Barramyia Gold Mine Area, Eastern Desert, Egypt. M.Sc. thesis, Faculty of Science, Assiut University, Assiut, p. 218P.
Abdelrady, M., et al., 2023a. Geophysical Investigations for the Identification of Subsurface Features Influencing Mineralization Zones. Journal of King Saud University-Science, 102809.
Abdelrady, M., et al., 2023b. Orogenic lode-gold Deposits and Listvenization Processes in the El-Barramiya Area, Eastern Desert, Egypt.
Abdelrady, M., et al., 2024. Application of the new edge filters of aeromagnetic data to detect the subsurface structural elements controlling the mineralization in the Barramiya area, in the Eastern Desert of Egypt. J. King Saud Univ. Sci., 103539
Abdelwahed, M., et al., 2024. Remote sensing and magnetic characterization of the Au mineralization and its structural implications: Meatiq dome, eastern desert, Egypt. J. Afr. Earth Sci., 105442
Abo Khashaba, S.M., et al., 2023. Application of remote sensing data integration in detecting mineralized granitic zones: a case study of the Gabal Al-Ijlah Al-Hamra, Central Eastern Desert, Egypt. J. Afr. Earth Sci. 200, 104855. https://doi.org/10.1016/J.JAFREARSCI.2023.104855.
Abu El-Leil, I., Mussa, M., 1984. Structural factors controlling rare metal occurrences at Igla-Barramiya area, Eastern Desert, Egypt. Ann. Geol. Surv. Egypt 14, 309–318.
Abubakar, F., et al., 2024. Evaluation of gold mineralisation potential using AHP systems and weighted overlay analysis. Sci. Rep. 14 (1), 21263.
Abudeif, A.M., et al., 2023. Geophysical prospecting of the Coptic monastery of Apa Moses using GPR and magnetic techniques: a case study, abydos, Sohag, Egypt. Sustainability 15 (14), 11119.
Ai, H., et al., 2024. Advancing potential field data analysis: the Modified Horizontal Gradient Amplitude method (MHGA). Contrib. Geophys. Geodes. 54 (2), 119–143.
Alarifi, S.S., et al., 2024. Remote sensing and aeromagnetic mapping for unveiling mineralization potential: nuqrah area, Saudi Arabia. Geomech. Geophys. Geo-energ. Geo-Resour. 10, 149.
Ali-Bik, M.W., et al., 2012. Serpentinite-hosted talc–magnesite deposits of Wadi Barramiya area, Eastern Desert, Egypt: characteristics, petrogenesis and evolution. J. Afr. Earth Sci. 64, 77–89.
Alrefaee, H., Soliman, M., 2023. Deducing the structural framework of the Southern Faghur-Siwa Basin, northern Western Desert, Egypt using potential field data. J. Afr. Earth Sci. 202, 104935.
Aprina, P.U., et al., 2024. Delineating geological structure utilizing integration of remote sensing and gravity data: a study from Halmahera, North Molucca, Indonesia. Vietnam J. Earth Sci. 46 (2), 147–167.
Arafa-Hamed, T., et al., 2023. Deep heat source detection using the magnetotelluric method and geothermal assessment of the Farafra Oasis, Western Desert, Egypt. Geothermics 109, 102648.
Araffa, S.A.S., et al., 2022. Integrated geophysical, remote sensing and geochemical investigation to explore gold-mineralizations and mapping listvenites at Wadi Haimur. Eastern Desert Egypt. Geocarto International 37 (2), 17565–17602.

Badawi, M., et al., 2022. Mapping structurally controlled alterations sparked by hydrothermal activity in the Fatira-Abu Zawal area, Eastern desert, Egypt. Acta Geol. Sinica - English Edition. https://doi.org/10.1111/1755-6724.15019.
Bohal, Y.M., et al., 2020. Application of upward continuation filter for geomagnetic data interpretation in Gondang, Bojonegoro area. J. Marine-Earth Sci. Technol. 1 (1), 1–7.
Chen, A.-G., et al., 2017. Application of an enhanced theta-based filter for potential field edge detection: a case study of the Luzong ore district. Chin. J. Geophys. 60 (2), 203–218.
Duong, N.T., et al., 2024. Identification of the active faults and seismotectonic zonation of Laos territory. Vietnam J. Earth Sci. 46 (4), 489–514.
Ejiga, G.E., et al., 2019. Utilizing the magnetic source edge detection (MSED) method in mapping geologic features within a sedimentary basin. Warta Geologi. 45 (3).
Ekinci, Y.L., et al., 2014. Geomagnetic and geoelectrical prospection for buried archaeological remains on the Upper City of Amorium, a byzantine city in midwestern Turkey. J. Geophys. Eng. 11 (1), 015012.
Ekinci, Y.L., et al., 2020. Geomagnetic Geophysical investigation of Mount Nemrut stratovolcano (Bitlis, Eastern Turkey) through aeromagnetic anomaly analyses. Pure Appl. Geophys. 177, 3243–3264.
El Saeed, R.L., et al., 2024. Economic feasibility of Gabal Um Takha leucogranitic intrusion, South Sinai, Egypt: integrated remote sensing, geochemical, aeromagnetic, and geotechnical approach. Phys. Chem. Earth Parts A/B/C 133, 103531.
El-Ela, A., 1985. AM Geology of Wadi Mubarak District, Eastern Desert, Egypt. Tanta University, Tanta Chicago, IL, USA. Ph. D. Thesis.
El-Gaby, S., et al., 1988. Geology, evolution and metallogenesis of the Pan-African belt in Egypt. The Pan-African Belt of Northeast Africa and Adjacent Areas: Tectonic Evolution and Economic Aspects of a Late Proterozoic Oregon.
Elkhateeb, S.O., et al., 2021. Probability of mineral occurrence in the Southeast of Aswan area, Egypt, from the analysis of aeromagnetic data. Arabian J. Geosci. 14, 1514.
Eldosouky, A.M., Saada, S.A., 2020. Source edge detection (SED) of aeromagnetic data: synthetic examples and a case study from Haimur area, south Eastern Desert, Egypt. Arabian J. Geosci. 13, 626.
Eldosouky, A.M., et al., 2022a. Mapping structural features of the Wadi Umm Dulfah area using aeromagnetic data. J. King Saud Univ. Sci. 34 (2), 101803.
Eldosouky, A.M., et al., 2022b. Structural interpretation of potential field data using the enhancement techniques: a case study. Geocarto Int. 37 (27), 16900–16925.
Eldosouky, A.M., et al., 2022c. High precision structural mapping using edge filters of potential field and remote sensing data: a case study from Wadi Umm Ghalqa area, South Eastern Desert, Egypt. Egypt J. Rem. Sens. Space Sci. 25, 501–513.
Eldosouky, A.M., et al., 2024a. Geological controls of mineralization occurrences in the Egyptian Eastern Desert using advanced integration of remote sensing and magnetic data. Sci. Rep. 14, 16700, 2024.
Eldosouky, A.M., et al., 2024b. A new vector for mapping gold mineralization potential and proposed pathways in highly weathered basement rocks using multispectral, radar, and magnetic data in random Forest algorithm. Nat. Resour. Res. 33, 23–50.
Eldosouky, A.M., et al., 2025. New insights into structural and tectonic evolution of Safaga-Semna shear belt, Eastern Desert, Egypt: advanced integration of aeromagnetic, remote sensing and field studies. Geomech. Geophys. Geo-energ. Geo-Resour. 11, 31.
Elhussein, M., et al., 2024. Aeromagnetic data analysis for sustainable structural mapping of the missiakat Al jukh area in the central Eastern desert: enhancing resource exploration with minimal environmental impact. Sustainability 16 (20), 8764.
Embaby, A., et al., 2024. Delineation of lineaments for groundwater prospecting in hard rocks: inferences from remote sensing and geophysical data. Environ. Earth Sci. 83 (2), 62.
Essa, K.S., et al., 2022. Aeromagnetic and radiometric data interpretation to delineate the structural elements and probable precambrian mineralization zones: a case study, Egypt. Mining Metall. Explor. 39 (6), 2461–2475.
Ferreira, F.J., et al., 2013. Enhancement of the total horizontal gradient of magnetic anomalies using the tilt angle. Geophysics 78 (3), J33–J41.
Fritz, H., et al., 2002. Neoproterozoic tectonothermal evolution of the Central Eastern Desert, Egypt: a slow velocity tectonic process of core complex exhumation. J. Afr. Earth Sci. 34 (3–4), 137–155.
Fu, J., et al., 2020. Combined magnetic, transient electromagnetic, and magnetotelluric methods to detect a BIF-Type concealed iron ore body: a case study in gongchangling iron ore concentration area, Southern Liaoning Province, China. Minerals 10 (12), 1044.
Gad, S., Kusky, T., 2006. Lithological mapping in the Eastern Desert of Egypt, the Barramiya area, using Landsat thematic mapper (TM). J. Afr. Earth Sci. 44 (2), 196–202.
Ghazala, H., et al., 2021. Integration of ASTER and geophysical data for delineating potential mineralization zones in Dungash-Atud area, Central Eastern Desert, Egypt. Arabian J. Geosci. 14, 1–22.
Ghoneim, S.M., et al., 2024. Integrating remote sensing and geophysical data for mapping potential gold mineralization localities at Abu Marawat area, central Eastern Desert, Egypt. Sci. Rep. 14 (1), 18273.
Ghosh, T., et al., 2022. Potential of ALOS-2 PALSAR-2 StripMap data for lithofacies identification and geological lineament mapping in vegetated fold-thrust belt of Nagaland, India. Adv. Space Res. 69 (4), 1840–1862. https://doi.org/10.1016/J.ASR.2021.09.007.
Gobashy, M.M., et al., 2022. Mapping of gold mineralization using an integrated interpretation of geological and geophysical data—A case study from West Baranes, South Eastern Desert, Egypt. Arabian J. Geosci. 15 (22), 1692.
Grauch, V., Cordell, L., 1987. Limitations of determining density or magnetic boundaries from the horizontal gradient of gravity or pseudogravity data. Geophysics 52 (1), 118–121.
Greiling, R., et al., 1994. A structural synthesis of the Proterozoic Arabian-Nubian Shield in Egypt. Geol. Rundsch. 83, 484–501.
Hamimi, Z., et al., 2023. Large-scale geological structures of the Egyptian Nubian shield. Sci. Rep. 13 (1), 1923.
Haralick, R.M., 1979. Statistical and structural approaches to texture. Proc. IEEE 67 (5), 786–804. https://doi.org/10.1109/PROC.1979.11328.
Hegab, M.A.E.-R., et al., 2022. Gold-related Alteration Zones Detection at the Um Balad Area, Egyptian Eastern Desert, using Remote Sensing, Geophysical, and GIS Data Analysis. J. Afr. Earth Sci. 196, 104715.
Hussien, H.M., 2023. Hydrogeological and remote sensing investigation of the fractured carbonate aquifer, East El Minia, Eastern Desert, Egypt. Groundw. Sustain. Dev. 23, 101006.
Ishola, K.S., et al., 2023. Groundwater potential mapping in hard rock terrain using remote sensing, geospatial and aeromagnetic data. Geosys. Geoenviron. 2 (1), 100107.
Issa, U., et al., 2021. Groundwater potential delineation using aeromagnetic data within sheet 223 Ilorin NW, South-western Nigeria. J. Nat. App. Sci. 10 (1), 1–8.
Jacobsen, B.H., 1987. A case for upward continuation as a standard separation filter for potential-field maps. Geophysics 52 (8), 1138–1148.
Johnson, P., et al., 2011. Late Cryogenian–Ediacaran history of the arabian–nubian shield: a review of depositional, plutonic, structural, and tectonic events in the closing stages of the northern East African Orogen. J. Afr. Earth Sci. 61 (3), 167–232.
Jorge, V.T., et al., 2023. A balanced edge detector for aeromagnetic data. Vietnam J. Earth Sci. 43 (3), 326–337.
Kamto, P.G., et al., 2023. Contribution of advanced edge detection flters for the structural mapping of the Douala Sedimentary Basin along the Gulf of Guinea. Vietnam J. Earth Sci. 43 (3), 287–302.
Kassia, G.V.S., et al., 2023. Structural features derived from a multi-method approach and 2.75 D modelling of aeromagnetic data: a case study of the Pitoa–Figuil area (Northern Cameroon). Acta Geophys. 71 (2), 587–600.
Klitzsch, E., 1986. Plate tectonics and cratonal geology in Northeast Africa (Egypt, Sudan). Geol. Rundsch. 75, 755–768.
Kroner, A., Stern, R., 2004. Pan-African orogeny. Encyclop. Geol. 1, 1–12.
Lghoul, M., et al., 2023. Application of enhanced methods of gravity data analysis for mapping the subsurface structure of the bahira basin in Morocco. Front. Earth Sci. 11, 1225714.
Li, N., et al., 2011. Textural and knowledge-based lithological classification of remote sensing data in Southwestern Prieska sub-basin, Transvaal Supergroup, South Africa. J. Afr. Earth Sci. 60 (4), 237–246. https://doi.org/10.1016/J.JAFREARSCI.2011.03.002.
Liem, N.V., et al., 2025. Advancing debris flow detection based on deep learning model and high-resolution images. Vietnam J. Earth Sci. 47 (2), 290–214.

McGrath, P.H., 1991a. Zero crossover – a Fortran program to determine the dip and extent of a geological boundary using horizontal derivatives of upward-continued gravity data. Comput. Geosci. 17, 1017–1031.
McGrath, P.H., 1991b. Dip and depth extend of density boundaries using horizontal derivatives of upward-continued gravity data. Geophysics 56, 1533–1542.
Melouah, O., et al., 2023. Lithospheric structural dynamics and geothermal modeling of the Western arabian Shield. Sci. Rep. 13, 11764.
Meshref, W., 1990. Tectonic framework of Egypt. In: Said, R. (Ed.), Geology of Egypt. Balkema/Rotterdam/Bookfield, Netherlands, pp. 113–156.
Miller, H.G., Singh, V., 1994. Potential field tilt—a new concept for location of potential field sources. J. Appl. Geophys. 32 (2–3), 213–217.
Mohamed, A., et al., 2022. Detection of mineralization zones using aeromagnetic data. Appl. Sci. 12 (18), 9078.
Nabighian, M.N., et al., 2005. The historical development of the magnetic method in exploration. Geophysics 70 (6), 33ND–61ND.
Nasuti, Y., Nasuti, A., 2018. NTilt as an improved enhanced tilt derivative filter for edge detection of potential field anomalies. Geophys. J. Int. 214, 36–45.
Nasuti, Y., et al., 2019. STDR: a novel approach for enhancing and edge detection of potential field data. Pure Appl. Geophys. 176, 827–841.
Obiora, D.N., et al., 2022. Comparative depth estimates and modeling of magnetic anomalies over the Nkalagu area, Southeastern Nigeria. Model. Earth Sys. Environ. 1–19.
Oksum, E., et al., 2021. A novel approach based on the fast sigmoid function for interpretation of potential field data. Bull. GeoPhys. ObServ. 62 (3), 543–556.
Oliveira, S.P., et al., 2023. On the practical implementation of the enhanced horizontal derivative filter for potential field data. Contrib. Geophys. Geodes. 53 (4), 319–331.
Othman, A.A., et al., 2024. Subsurface structure delineation using gravity and magnetic data interpretation at the area South Gebel miswag, Northwestern desert, Egypt. Egypt. J. Geol.
Pham, L.T., 2024a. An improved edge detector for interpreting potential field data. Earth Sci. Inform. 17 (3), 2763–2774.
Pham, L.T., 2024b. A stable method for detecting the edges of potential field sources. IEEE Trans. Geosci. Rem. Sens. 62, 1–7.
Pham, L.T., Prasad, K.N.D., 2023. Analysis of gravity data for extracting structural features of the northern region of the Central Indian Ridge. Vietnam J. Earth Sci. 45 (2), 147–163.
Pham, L.T., et al., 2022a. A new high resolution filter for source edge detection of potential field data. Geocarto Int. 37 (11), 3051–3068.
Pham, L.T., et al., 2022b. A comparative study on the peak detection methods used to interpret potential field data: a case study. Geocarto Int. 37 (13), 3679–3696.
Pham, L.T., et al., 2024. Reliable Euler deconvolution solutions of gravity data throughout the β-VDR and THGED methods: application to mineral exploration and geological structural mapping. Vietnam J. Earth Sci. 46 (3), 432–448.
Pham, L.T., et al., 2025. Enhancing potential fields using stable downward continuation and boundary filters: application to the Central highlands. Vietnam J. Earth Sci. 47 (2), 236–251.
Prasad, K.N.D., et al., 2022. Structural mapping of potential field sources using BHG filter. Geocarto Int. 37 (26), 11253–11280.
Raju, P.S., Kumar, K.S., 2020. Magnetic survey for iron-oxide-copper-gold (IOCG) and alkali calcic alteration signatures in Gadarwara, MP, India: implications on copper metallogeny. Minerals 10 (8), 671.
Reid, A.B., et al., 1990. Magnetic interpretation in three dimensions using Euler deconvolution. Geophysics 55 (1), 80–91.
Ries, A.C., et al., 1983. Pan-African structures, ophiolites and mélange in the Eastem Desert of Egypt: a traverse at 26 N. J. Geol. Soc. 140 (1), 75–95.
Roest, W.R., et al., 1992. Magnetic interpretation using the 3-D analytic signal. Geophysics 57 (1), 116–125.
Saada, S.A., 2016. Edge detection and depth estimation of Galala El Bahariya Plateau, Eastern Desert-Egypt, from aeromagnetic data. Geomech. Geophys. Geo-energ. Geo-Resour. 2, 25–41.
Saada, S.A., 2022. Understanding the structural framework controlling the sedimentary basins from the integration of gravity and magnetic data: a case study from the east of the Qattara Depression area, Egypt. J. King Saud Univ. Sci. 34 (2022), 101808.
Saada, S.A., et al., 2021a. New insights into the contribution of gravity data for mapping the lithospheric architecture. J. King Saud Univ. Sci. 33, 101400.
Saada, S.A., et al., 2021b. Insights on the tectonic styles of the Red Sea rift using gravity and magnetic data. Mar. Petrol. Geol. 264–8172.
Saada, S.A., et al., 2025. Insights on the structural framework of the Egyptian Eastern Desert derived from edge detectors of gravity data. Interpretation 13, T71–T85.
Said, R., 1962. The Geology of Egypt. Elsevier Publishing Co., Amsterdam-New York, p. 337.
Saleh, A., et al., 2018. Subsurface structural features of the basement complex and mineralization zone investigation in the Barramiya area, Eastern Desert of Egypt, using magnetic and gravity data analysis. Arabian J. Geosci. 11, 1–14.
Salem, S., et al., 2014. Exploration of new gold occurrences in the alteration zones at the Barramiya District, Central Eastern Desert of Egypt using ASTER data and geological studies. Arabian J. Geosci. 7, 1717–1731.
Salem, S., et al., 2016. Exploration of gold occurrences in alteration zones at Dungash district, Southeastern Desert of Egypt using ASTER data and geochemical analyses. J. Afr. Earth Sci. 117, 389–400.
Schandelmeier, H., et al., 1987. Structural Development of north-east Africa Since Precambrian Times.
Sehsah, H., Eldosouky, A.M., 2020. Neoproterozoic hybrid forearc – MOR ophiolite belts in the northern Arabian-Nubian shield: no evidence for back-arc tectonic setting. Int. Geol. Rev. 64 (2), 151–163.
Sehsah, et al., 2019. Unpaired ophiolite belts in the Neoproterozoic Allaqi-Heiani Suture, the Arabian-Nubian Shield: evidences from magnetic data. J. Afr. Earth Sci. 156, 26–34.
Shebl, A., et al., 2023. Towards better delineation of hydrothermal alterations via multi-sensor remote sensing and airborne geophysical data. Sci. Rep. 13 (1), 7406.
Shebl, A., Csámer, Á., 2021. Reappraisal of DEMs, Radar and optical datasets in lineaments extraction with emphasis on the spatial context. Remote Sens. Appl.: Soc. Environ. 24, 100617. https://doi.org/10.1016/J.RSASE.2021.100617.
Shebl, A., et al., 2021. Multisource data analysis for gold potentiality mapping of atalla area and its environs, central Eastern desert, Egypt. Minerals 11 (6), 641.
Shebl, A., et al., 2024. Novel comprehensions of lithological and structural features gleaned via Sentinel 2 texture analysis. Ore Geol. Rev. 168, 106068. https://doi.org/10.1016/j.oregeorev.2024.106068.
Shukri, N., Lotfi, M., 1955. The geology of the Bir Barramiya area. Bull. Fac. Sci. Cairo Univ. 34, 83–130.
Stern, R., 1994. Neoproterozoic (900-550 Ma) arc assembly and continental collision in the East Africa orogen: implications for the consolidation of Gondwanaland. Annu. Rev. Earth Planet Sci. 22, 319–351.
Sturchio, N.C., et al., 1983. Geology and origin of Meatiq Dome, Egypt: a Precambrian metamorphic core complex? Geology 11 (2), 72–76.
Thao, N.T.P., et al., 2023. Monitoring the storage volume of impounding reservoirs in inaccessible regions using multi-sensor satellite data: the case study of Tuyen Quang Reservoir (Vietnam). Vietnam J. Earth Sci. 45 (2), 199–218.
Toushmalani, R., et al., 2024. A well-structured metaheuristic optimization technique for magnetic data inversion of 2D dipping dyke-like geological structures using the cuckoo optimization algorithm. Arabian J. Sci. Eng. 1–10.
Wijns, C., et al., 2005. Theta map: edge detection in magnetic data. Geophysics 70 (4), L39–L43.
Zhdanov, M.S., 2021. Editorial for special issue "Geophysics for Mineral Exploration". MDPI 11, 692.
Zoheir, B., et al., 2019. Orogenic gold in transpression and transtension zones: field and remote sensing studies of the barramiya–mueilha sector, Egypt. Remote Sens. 11 (18), 2122.
Zoheir, B.A., Akawy, A., 2010. Genesis of the Abu Marawat gold deposit, central Eastern Desert of Egypt. J. Afr. Earth Sci. 57 (4), 306–320.